Journal of Catalysis **193,** 5–15 (2000)
doi:10.1006/jcat.2000.2879, available online at http://www.idealibrary.com on IDEAL®

Effect of Surface Treatment of the Support on CO Oxidation over Carbon-Supported Wacker-Type Catalysts

Eun Duck Park and Jae Sung Lee[1]

Department of Chemical Engineering and School of Environmental Engineering, Pohang University of Science and Technology (POSTECH), San 31 Hyoja Dong, Pohang 790-784, Republic of Korea

Received June 4, 1999; revised March 24, 2000; accepted March 28, 2000

The effect of surface treatment of the support on the oxidation of carbon monoxide over carbon-supported Wacker-type catalysts was examined. Temperature-programmed desorption (TPD) and FT-IR were used to characterize the surface functional groups of carbon. XRD patterns and XAFS spectra of the catalysts were measured to determine the structure and the chemical environment of palladium and copper. Carboxylic and carbonyl groups were enriched on the carbon support by the pretreatment of the support with HNO_3 or the addition of $Cu(NO_3)_2$ as a copper precursor. These surface groups increased the hydrophilicity determined by H_2O-TPD, and promoted the formation of active copper phase, $Cu_2Cl(OH)_3$. This appears to be responsible for the observed promotional effect on CO oxidation when $Cu(NO_3)_2$ was added as an additional copper precursor.

Key Words: **CO oxidation; Wacker-type catalyst; carbon; acid treatment; XRD; XAFS.**

INTRODUCTION

The Wacker catalyst, homogenous $PdCl_2$–$CuCl_2$ dissolved in water, has been used in industry to produce acetaldehyde from ethylene (1, 2). To overcome the drawbacks of this classic process, including the corrosion problem, heterogenized Wacker-type catalysts have been proposed (3, 4). This heterogenized catalyst system has also been reported to oxidize carbon monoxide at ambient temperatures in the presence of water (5–17). Compared with other low-temperature CO oxidation catalysts such as hopcalite, supported Au catalysts, and Pt/SnOx, this supported Wacker-type catalyst system was found to be stable even in the presence of organic halogen compounds in the feed. This advantage led to establishment of a new process which oxidizes CO at a low temperature (<420 K) in the presence of water and halogen compounds (17).

In the supported $PdCl_2$–$CuCl_2$ catalyst system, the characteristic of the support is a critical parameter for its catalytic performance. Choi and Vannice (7) observed a higher activity over hydrophobic carbon than over hydrophilic alumina. They also discussed the water effect over these two different supports. Lee *et al.* (8) reported that the catalytic activity decreased approximately in the order active carbon > (active carbon + zeolite) > ZSM-5 > MS-13X > MS-5A > alumina. Kim *et al.* (9) reported that the activity of alumina-supported $PdCl_2$–$CuCl_2$ showed a marked dependence on the partial pressure of water whereas the carbon-supported catalyst showed no such dependence, although its presence was still required.

Lloyd and Rowe (10) have claimed that $Cu(NO_3)_2$ serves as a promoter for this catalyst when supported on alumina and used for CO oxidation. Kim *et al.* (9) examined the effect of catalyst composition and reaction conditions.

There have been a number of works on characterization of supported $PdCl_2$–$CuCl_2$ catalysts. Choi and Vannice (7) investigated the mechanism of CO oxidation by kinetic and IR studies. They suggested that the active species on the catalyst surface were PdClCO, CuClCO, and possibly a Pd–Cu complex. From the X-ray absorption fine structure (XAFS) study, Lee *et al.* (11, 12) examined the $PdCl_2$–$CuCl_2$/Al_2O_3 catalysts and found that the active phase of palladium was Pd(II) species containing Cl and possibly carbonyl ligands. No direct interaction of Pd–Pd or Pd–Cu was observed. The active phase of copper was suggested to be solid $Cu_2Cl(OH)_3$ particles.

Recently, we found that the catalytic activity of the supported Wacker-type catalyst was closely related to the solid phase of Cu (14–16). $Cu_2Cl(OH)_3$ was found to be the most active copper phase and its peak intensity in XRD was proportional to the catalytic activity. This might be related to the ease of reduction for the $Cu_2Cl(OH)_3$ phase compared with other Cu(II) species as revealed by the appearance of the TPR peak at a lower temperature (18). Zepelli *et al.* (19) suggested that basic hydroxyl groups might be involved in the formation of $Cu_2Cl(OH)_3$ over Al_2O_3. To improve the catalytic activity of supported Wacker-type catalyst, stable $Cu_2Cl(OH)_3$ should be formed over proper supports. Activated carbon has been reported to be superior to other

[1] To whom correspondence should be addressed. Fax: 82-562-279-5799. E-mail: jlee@postech.ac.kr.

0021-9517/00 $35.00

supports for the supported Wacker-type catalysts and can also be modified chemically to have an oxidative surface character by using various techniques (20). Of the oxidative modification techniques reported, nitric acid oxidation is best known. The main purpose of oxidation of the carbon surface is to obtain a more hydrophilic surface with a relatively large number of oxygen-containing surface groups. The chemical character of the activated surface is determined basically by the amount of chemically bound oxygen and the structure of the surface bonds (number and type of functional groups). In studies of the chemistry of such surfaces, thermal analysis and IR spectroscopy techniques have been frequently used (20–27). In the present paper, the effect of the chemical properties of activated carbon on CO oxidation over supported $PdCl_2$–$CuCl_2$ and $PdCl_2$–$CuCl_2$–$Cu(NO_3)_2$ catalysts was examined.

EXPERIMENTAL

Preparation of Support

Two kinds of carbon supports were used to determine the effect of surface functional groups on CO oxidation. Activated carbon (AC) was obtained from Aldrich and its particulate size was 20–40 mesh. Surface–modified activated carbon (M-AC) was prepared by acid treatment. Thus, the activated carbon was treated with 7 N HNO_3 at 353 K for 3 h, washed with distilled water, and dried at 423 K for 12 h to remove the remaining nitric acid. The BET surface areas and pore volumes of these two supports are presented in Table 1.

Preparation of Catalyst

The catalyst was prepared by a wet impregnation method to impregnate supports with an aqueous solution of palladium and copper. The support was dried at 423 K for 12 h in an oven before impregnation. The metal precursors were $PdCl_2$ (Sigma, 99.9%), $CuCl_2 \cdot 2H_2O$ (Aldrich, 99.9%), and $Cu(NO_3)_2 \cdot 3H_2O$ (Aldrich, 99.9%). Four kinds of supported Wacker-type catalysts were prepared as described in Table 2. The loadings of Pd and Cu for all catalysts were 2 wt% and 12 wt%, respectively, and the mole ratio of $CuCl_2$ to $Cu(NO_3)_2$ was 1 : 2 for $PdCl_2$–$CuCl_2$–$Cu(NO_3)_2$ catalysts. The chlorine content was 12 wt% for WA-1 and WA-2 catalysts and and 3 wt% for WA-3 and WA-4 catalysts. The BET surface areas for these four catalysts are listed in Table 2. All catalysts were stored under ambient conditions and there was no pretreatment before the reaction unless specified.

TABLE 1

N_2 Adsorption Data for Fresh Activated Carbon and the HNO_3-Treated Activated Carbon

Support	BET surface area, m^2/g	Micropore volume,[a] cm^3/g	Micropore area,[a] m^2/g
AC	689.9	0.12	261.1
M-AC	679.5	0.13	288.9

[a] Obtained from *t*-plot.

TABLE 2

BET Surface Area of Different Wacker-Type Catalysts

Catalyst	Description	BET surface area, m^2/g
WA-1	$PdCl_2$–$CuCl_2$/AC	207.9
WA-2	$PdCl_2$–$CuCl_2$/M-AC	217.9
WA-3	$PdCl_2$–$CuCl_2$–$Cu(NO_3)_2$/AC	206.1
WA-4	$PdCl_2$–$CuCl_2$–$Cu(NO_3)_2$/M-AC	215.0

CO Oxidation

The rates of CO oxidation were measured in a small fixed-bed reactor with catalysts of 100/120 mesh. The reaction temperature was monitored by use of a thermocouple inserted into the center of the catalyst bed. A premixed feed of 1 vol% CO and 10 vol% O_2 in nitrogen was supplied through a mass flow controller into the reactor. The feed stream was saturated with water through a saturator enclosed in a constant temperature bath and fed to the reactor. The constant reaction temperature of the reactor was achieved by controlling the temperature of an electric furnace surrounding the reactor. Reactants and products were analyzed by online gas chromatography (HP5890A, molecular sieve 13X column). All reaction rates were obtained under differential reaction conditions where the conversions of CO were kept below 10–15%.

Characterization of Catalysts

Temperature-programmed desorption (TPD). Samples were pretreated with He at 323 K for 1 h before being weighed. TPD was conducted in a He stream from 303 K to 1303 K at a heating rate 10 K min^{-1} monitoring gas products with a mass-selective detector (HP5971 MSD). In the case of H_2O-TPD, water adsorption was made over a 50-mg sample in the quartz reactor at 313 K by flowing a He stream saturated with water at 293 K for 30 min prior to TPD experiments.

FT-IR. FTIR spectra of AC and M-AC in the transmission mode were obtained with a Perkin Elmer IR spectrophotometer (Model 1800) using pellets of KBr containing about 0.6% of carbon. These pellets were dried overnight at 373 K before the spectra were recorded. The reference spectrum was the open-beam mirror background spectrum. The original spectra were corrected with a curved baseline, used for strongly scattering samples (24).

X-ray diffraction (XRD). X-ray powder diffraction patterns were obtained at room temperature using an

M18XHF (MAC Science Co.) with Ni-filtered Cu $K\alpha$ radiation (1.54056 Å). The X-ray tube was operated at 40 kV and 200 mA. Samples were finely ground and packed into a glass holder having an 18- × 18- × 2-mm opening. No adhesive or binder was necessary. The 2θ angle was scanned at a rate of 4° min^{-1}.

X-ray absorption fine structure (XAFS). The XAFS spectra were taken in a transmission mode for K-edge of Cu and Pd at beamline 10 B of the Photon Factory in Tsukuba, Japan. The photon energies were calibrated using a Cu K-edge energy at 8979.0 eV for Cu metal. Spectra for the Pd sample were obtained at room temperature without exposing the samples to air using a controlled atmosphere EXAFS cell with Kapton windows (11, 12). However, in the case of Cu samples, it was difficult to make such a thin EXAFS powder cell because of high Cu loading. Thus, Cu samples in a controlled atmosphere EXAFS cell were exposed to air just before the measurement to minimize the exposure time. The obtained XANES (X-ray absorption near-edge structure) spectra were analyzed in a VAX/VMS operating system by using the UW5 package, and EXAFS (extended X-ray absorption fine structure) data were analyzed by using the UWXAFS 3.0 package (28) and FEFF 7.0 code (29), both licensed from the University of Washington. The standard analysis procedure is described elsewhere in detail (30).

The nonlinear EXAFS fitting was performed in R-space without Fourier filtering. The standards were Pd–Pd and Pd–Cl single scatterings that were synthesized with the FEFF code by using structural information for Pd metal (31) and $PdCl_2$ (32). A single adjustable parameter in XAFS analysis, the amplitude reduction factor (S_0^2), was taken to be 0.88 for Pd, which was found by fitting the experimental RSF of Pd foil with the theoretical one.

RESULTS

The physical properties were measured for the fresh activated carbon (AC) and the modified activated carbon (M-AC) prepared by the nitric acid treatment. These two carbon supports have almost the same BET surface area as shown in Table 1. Other N_2 adsorption data such as pore size distribution (PSD) and the shape of the adsorption–desorption isotherms were also similar. Hence, modification has been successfully made without disrupting the original texture of AC.

FT-IR spectra were obtained to observe the difference in the surface functional groups of carbon supports before and after treatment with HNO_3. Fresh activated carbon has a broad envelope over 1000–1300 cm^{-1} and a small band at 1580 cm^{-1} as shown in Fig. 1. Upon treatment with HNO_3, the intensity of bands observed in the fresh activated carbon was strengthened and new bands appeared. A band at 1210 cm^{-1} is developed as a shoulder to the original band

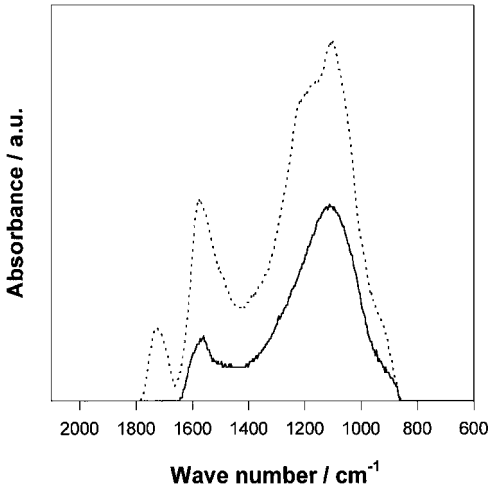

FIG. 1. Baseline-corrected FT-IR spectra of fresh activated carbon (AC, solid line) and activated carbon after HNO_3 treatment (M-AC, dotted line).

at 1100 cm^{-1} and another new band appears at 1750 cm^{-1}. From the previous IR studies (25–27) on surface functional groups of carbon, bands at 1100–1450, 1580, and 1550–2050 cm^{-1} could be related to C–O stretching, polyaromatic C=C stretching, and C=O stretching modes, respectively. Hence, surface oxygen groups are enriched and diversified over activated carbon upon treatment with HNO_3.

Temperature-programmed desorption (TPD) was also conducted to observe the change in surface functional groups and their hydrophilicity. In H_2O-TPD, Fig. 2a shows

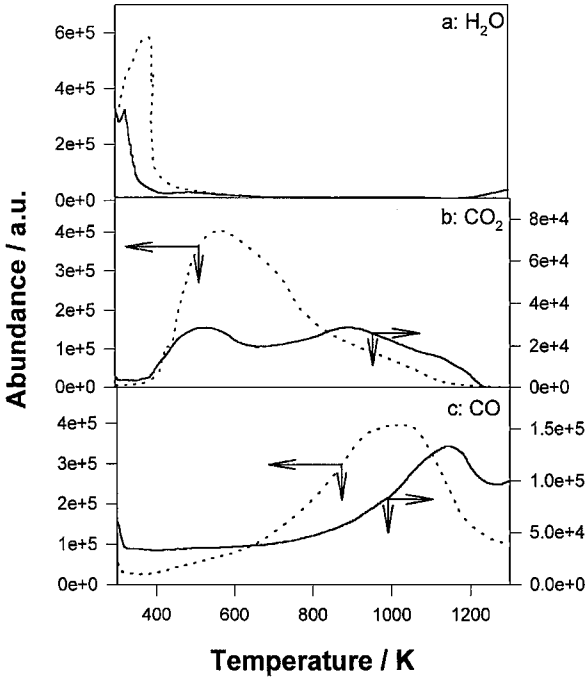

FIG. 2. H_2O–TPD patterns of fresh activated carbon (solid line) and activated carbon after HNO_3 treatment (dotted line).

that the amount of desorbed H_2O increases and its peak maximum shifts to a higher temperature after activated carbon is modified with HNO_3. Thus, the fresh activated carbon has an H_2O peak maximum at 320 K and the modified activated carbon at 380 K. The amount of desorbed CO_2 from the modified activated carbon is much greater than that from the fresh activated carbon as shown in Fig. 2b. The fresh activated carbon shows two CO_2 peaks with maxima of 520 K and 900 K. However, the modified activated carbon has a single maximum at 560 K and a shoulder at 720 K. The amount of desorbed CO increases and the peak maximum shifts to a lower temperature after the modification of the activated carbon as shown in Fig. 2c. The fresh activated carbon has a single maximum at 1140 K and the modified activated carbon shows two CO peaks with maxima of 960 K and 1040 K. It is well accepted that surface functional groups, derived from carboxylic acids such as anhydrides, lactones, and the acids themselves, yield predominantly CO_2 upon decomposition, whereas CO is formed during the decomposition of functional groups containing one oxygen atom (20–24). A consequence of having enriched surface groups such as carbonyl and carboxyl is the increase in the hydrophilicity as revealed in Fig. 2a by the enhanced water adsorption.

To determine the effects of surface functional groups of carbon supports on CO oxidation over carbon-supported Wacker-type catalysts, four kinds of catalysts were prepared as described in Table 2 and were denoted as WA-1 to WA-4. Their BET surface areas were almost the same. The rates of CO oxidation over WA-1, WA-2, WA-3, and WA-4 at 313 K and 353 K are shown in Fig. 3. The reaction rates are expressed in moles of CO converted per mole of Pd per second. They are true turnover rates because Pd was found to be the main active component of the catalyst (7, 9, 14, 15) and to be present as a molecular species containing a single Pd atom as shown later in the XAFS study. Supported $PdCl_2$–$CuCl_2$ catalysts such as WA-1 and WA-2 showed stable activities at 313 K from the start, but the catalytic activities of supported $PdCl_2$–$CuCl_2$–$Cu(NO_3)_2$ catalysts such as WA-3 and WA-4 started low, increased progressively, reached a maximum, and decreased slightly to reach steady-state values. WA-4 needed a longer time to reach the steady-state activity than WA-3. The rates of CO oxidation over WA-1, WA-2, WA-3, and WA-4 at 353 K are also shown in Fig. 3b. The catalytic activities of supported $PdCl_2$–$CuCl_2$ catalysts such as WA-1 and WA-2 increased progressively and reached the steady states, and the catalytic activities of supported $PdCl_2$–$CuCl_2$–$Cu(NO_3)_2$ catalysts such as WA-3 and WA-4 increased at first but decreased steadily to reach the steady states. Catalysts made of the modified activated carbon also showed higher activities than those with the unmodified support at steady state both at 313 K and at 353 K for all catalysts. The induction period for the supported $PdCl_2$–$CuCl_2$–$Cu(NO_3)_2$ catalyst was found to be shortened by pretreatment with dinitrogen at elevated temperatures

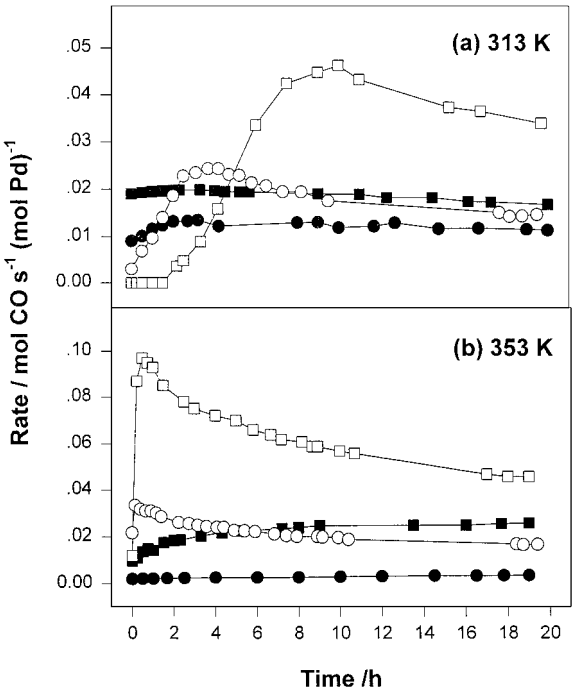

FIG. 3. Rate of CO oxidation over WA-1 (●), WA-2 (■), WA-3 (○), and WA-4 (□) at 313 K and at 353 K. The reactants, CO, O_2, and H_2O, were fed to the catalyst at concentrations of 1 vol%, 10 vol%, and 2.3 vol% each in nitrogen.

as shown in Fig. 4. But the steady-state activity for the catalyst pretreated at 473 K was lower compared with those for other catalysts pretreated at lower temperatures. TPD was conducted to determine the effect of pretreatment for supported $PdCl_2$–$CuCl_2$–$Cu(NO_3)_2$ catalysts. Figure 5a shows that the amounts of desorbed CO_2 from both catalysts are

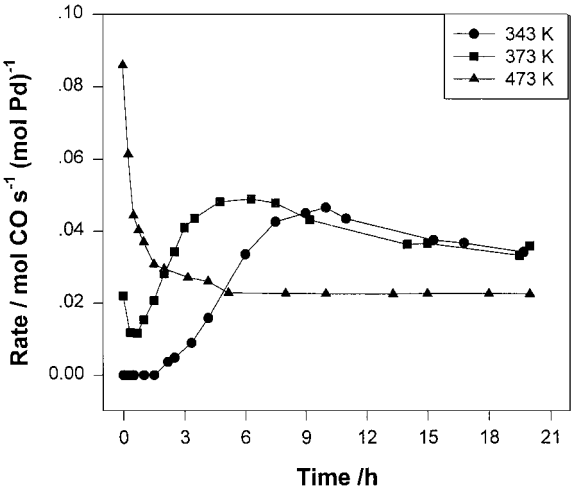

FIG. 4. Rate of CO oxidation at 313 K over WA-4 pretreated with nitrogen at different temperatures. The reactants, CO, O_2, and H_2O, were fed to the catalyst at concentrations of 1 vol%, 10 vol%, and 2.3 vol% each in nitrogen.

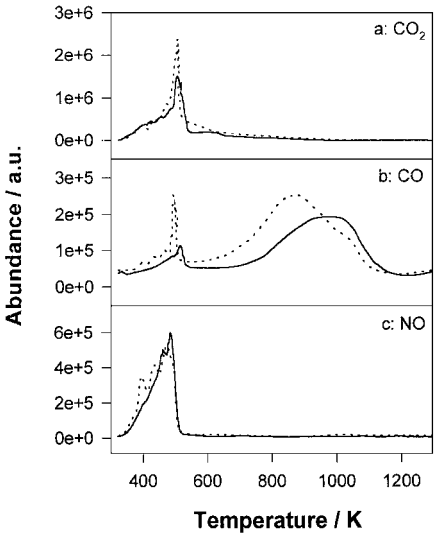

FIG. 5. TPD patterns of $PdCl_2$–$CuCl_2$–$Cu(NO_3)_2$ catalysts supported on unmodified (solid line) and modified activated carbon (dotted line).

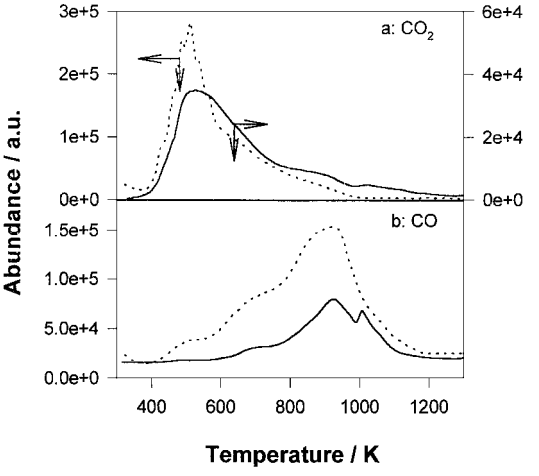

FIG. 6. TPD patterns of $PdCl_2$–$CuCl_2$ catalysts supported on unmodified (solid line) and modified activated carbon (dotted line).

much greater than those from supports themselves shown in Fig. 2b. WA-3 and WA-4 have a single maximum of CO_2 evolution at 500 K, whereas the amount of desorbed CO_2 from WA-4 is greater than that from WA-3. The amounts of desorbed CO are also greater for these catalysts as shown in Fig. 5b compared with those from supports shown in Fig. 2c. WA-3 has CO peaks at 500 K and a broad peak over 900–1000 K. WA-4 has CO peaks with maxima at 500 K and 880 K. For both cases, the CO peak at 500 K is caused by splitting of CO_2 during the mass detection process because the intensity ratio between CO and CO_2 peaks is identical to that of reference CO_2 and the temperature and the shape of the two peaks are identical. Thus, these CO peaks at 500 K have not been produced from catalysts. Figure 4c shows that NO is removed completely at 520 K for both catalysts. For comparison, TPD was also conducted for supported $PdCl_2$–$CuCl_2$ catalysts. Figure 6a shows that the amounts of desorbed CO_2 from WA-1 ($PdCl_2$–$CuCl_2$/AC) or WA-2 ($PdCl_2$–$CuCl_2$/M-AC) catalysts are a little less than those from supports themselves shown in Fig. 2b. WA-1 has a broad peak over 520–530 K and WA-2 a sharper peak at 510 K. Compared with Fig. 2b, the peak at 900 K and the shoulder at 720 K observed in supports themselves disappeared for WA-1 and WA-2, respectively. These peaks are related to carboxylic anhydrides which are adjacent acidic oxygen complexes formed at dangling carbon sites (23). WA-1 has two CO peaks at 930 K and 1000 K. WA-2 has a single peak at 920 K. Compared with supports alone, peaks at 1140 K and 1040 K disappeared from AC and M-AC, respectively, when $PdCl_2$–$CuCl_2$ was loaded. These peaks are related to ether, quinone, and hydroquinone groups (21, 22). Thus, employment of $Cu(NO_3)_2$ as a copper precursor has changed the population and nature of surface oxygen groups of activated carbon. Enrichment of carboxyl groups is particularly conspicuous as evidenced by greatly increased CO_2 evolution in TPD of WA-3 and WA-4.

We reported that the XRD peak intensity of $Cu_2Cl(OH)_3$ was closely related to the catalytic activity for supported Wacker-type catalysts (14, 15). Thus, XRD patterns of these catalysts before and at maximum activities at 353 K are shown in Fig. 7. No peaks related to Pd species can be

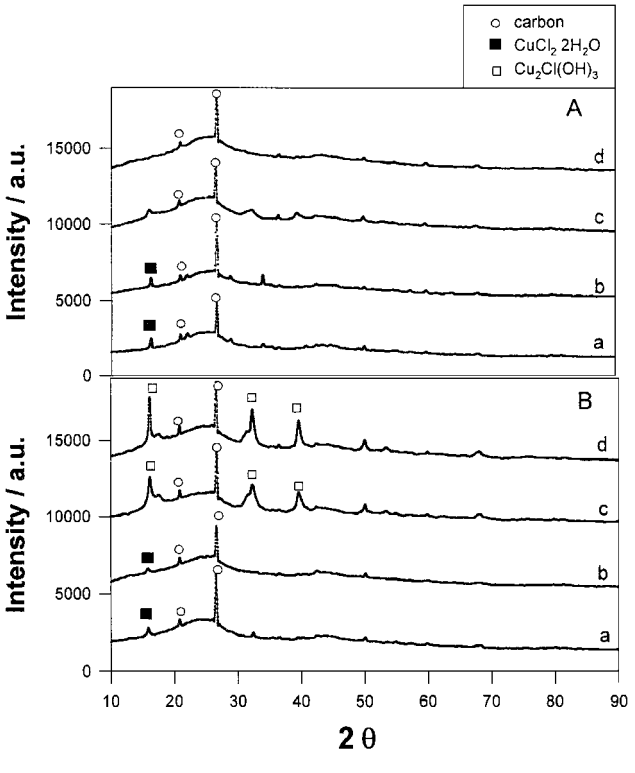

FIG. 7. X-ray diffractogram of WA-1 (a), WA-2 (b), WA-3 (c), and WA-4 (d) before the reaction (A) and at points of maximum activities at 353 K (B).

observed. In addition to peaks due to the support, only peaks representing $Cu_2Cl(OH)_3$ and $CuCl_2 \cdot 2H_2O$ are observed with different intensities. Supported $PdCl_2$–$CuCl_2$ catalysts show a weak intensity of the $CuCl_2 \cdot 2H_2O$ phase before and after reaction at 353 K. This indicates that surface functional groups do not promote effectively the formation of an active copper phase, $Cu_2Cl(OH)_3$, for these catalysts. Supported $PdCl_2$–$CuCl_2$–$Cu(NO_3)_2$ catalysts show a weak intensity of the copper phase before reaction. However, the peak intensities representing the $Cu_2Cl(OH)_3$ phase have increased at maximum activities and a stronger peak intensity is observed over M-AC than over AC.

In order to obtain information on the chemical states of Pd and Cu species in these catalysts after reaction at 353 K, the technique of X-ray absorption near-edge structure (XANES) was employed. Figure 8 compares Pd K-edge XANES of these catalysts before the reaction (a) and at the points of maximum activities (b) at 353 K with those of some reference compounds, Pd foil, $PdCl_2$, and $Pd(NO_3)_2$. The maximum absorption edge in each spectrum corresponds to the allowed $1s \rightarrow 5p$ transition. Pd references show easily differentiated shapes of their respective XANES. All catalysts before and during the reaction at 353 K show XANES shapes similar to that of $PdCl_2$. The XANES also provides the edge position, which is directly related to the binding energy of the ejected electron during the absorption process. It moves to a higher energy as the oxidation state of the absorbing atom increases. The

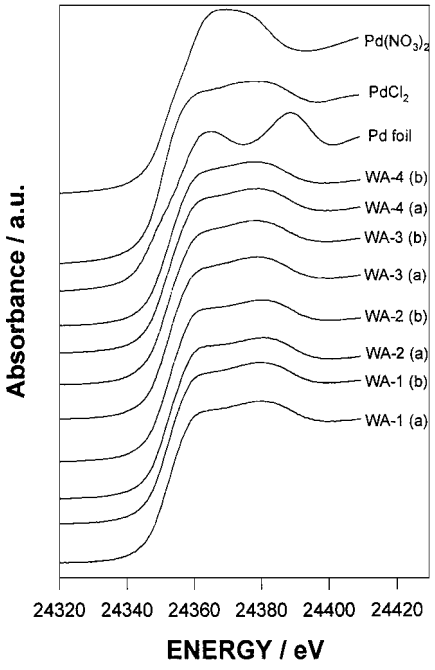

FIG. 8. Pd K-edge XANES of WA-1, WA-2, WA-3, and WA-4 before reaction (a) and at points of maximum activities at 353 K (b). Pd references are also given.

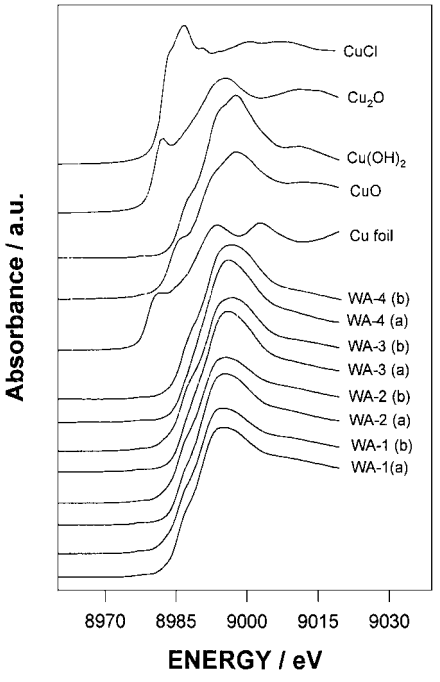

FIG. 9. Cu K-edge XANES of WA-1, WA-2, WA-3, and WA-4 before reaction (a) and at points of maximum activities at 353 K (b). Cu references are also given.

edge positions determined for Pd foil, $PdCl_2$, and $Pd(NO_3)_2$ were 24348.0 eV, 24351.0 eV, and 24351.5 eV, respectively, and again reflected the shift to a higher energy as the oxidation number was raised. For all catalysts, the edge energy positions were determined to be between 24350.9 eV and 24353.2 eV, which could be assigned to Pd(II) compounds. Thus, it was found that Pd was present as $PdCl_2$ in all catalysts before and after the reaction at 353 K. In the case of Cu species, Fig. 9 compares Cu K-edge XANES of these catalysts before the reaction (a) and at the points of maximum activities (b) at 353 K with those of some reference compounds, Cu foil, CuO, $Cu(OH)_2$, Cu_2O, and CuCl. As discussed elsewhere (11, 12, 15), the absorbance maximum is assigned to the allowed $1s \rightarrow 4p$ transition. Below the maximum, there are subsidiary peaks and shoulders reflecting transitions to empty orbitals according to the dipole selection rule (11, 12, 15). A very weak peak below the edge at 8978 eV in CuO and $Cu(OH)_2$ represents the quadruple-allowed $1s \rightarrow 3d$ transition, which serves as a signature of a Cu(II) compound since there is no $3d$ hole in Cu(0) or Cu(I) compounds. These very weak peaks are also found for all catalysts before and during the reaction at 353 K. Therefore, a majority of copper species present for these catalysts seems to be Cu(II) compounds. The $1s \rightarrow 4s$ peak in Cu(II) compounds appears at 8985 eV as a shoulder with greatly reduced intensity. The edge positions of these references were determined to be 8979.0 eV, 8984.6 eV, 8986.3 eV, 8981.0 eV, and 8982.5 eV for Cu foil, CuO, $Cu(OH)_2$, Cu_2O, and CuCl, respectively, and again reflected the shift to a

higher energy as the oxidation number increased. For all catalysts before and during the reaction at 353 K, the edge energy positions are determined to be between 8985.7 eV and 8987.0 eV, corresponding to Cu(II) compounds. Thus, all catalysts observed before the reaction (spectra a in Fig. 9) and at the points of the maximum activity at 353 K (spectra b in Fig. 9) contained Cu(II) species. Yet, both catalysts showed a broad maximum in absorbance unlike any other reference copper compounds. This tendency was more distinct for catalysts working at maximum activities. General features of these XANES spectra are similar to ones previously observed for $PdCl_2$–$CuCl_2$/Al_2O_3 catalysts that were active in CO oxidation, except the doublet maxima observed for the alumina-supported catalysts (11, 12) instead of one broad maximum as observed here.

In order to obtain information on the structural change of Pd species in these catalysts supported on different carbon supports, the technique of extended X-ray absorption fine structure (EXAFS) was employed. First, EXAFS functions weighted with k^3 and their radial structural function (RSF) for carbon-supported $PdCl_2$–$CuCl_2$ catalysts before and after the reaction at 353 K are displayed in Fig. 10. Only one

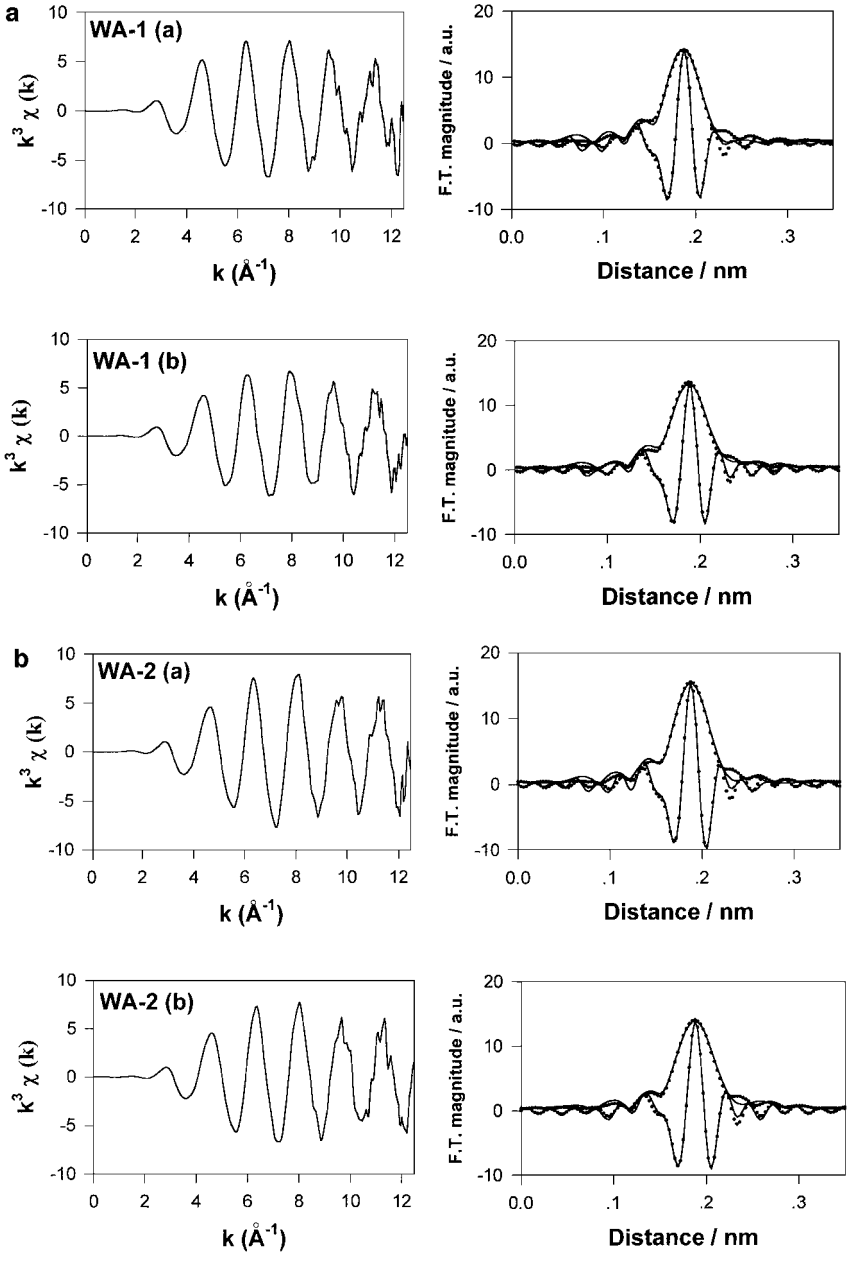

FIG. 10. k^3-weighted EXAFS functions and their Fourier transformation about the Pd K-edge of WA-1 and WA-2 before (a) and after the reaction at 353 K (b). The best-fit results are also plotted in dots.

TABLE 3

Pd K-Edge EXAFS Curve-Fitting Results of Carbon-Supported Wacker-Type Catalysts before (a) and after the Reaction at 353 K (b)

Catalyst	Shell	N	R (Å)	σ^2 (Å^2)	R-factor[a]
WA-1(a)	Cl	4.05	2.310	0.0036	0.0129
WA-1(b)	Cl	3.55	2.316	0.0029	0.0095
WA-2(a)	Cl	4.02	2.311	0.0029	0.0123
WA-2(b)	Cl	3.77	2.317	0.0075	0.0071

[a] The R-factor gives a sum-of-squares measure of the fractional misfit, which is defined as $R = \sum_{i=1}^{N}\{[Re(f_i)]^2 + [Im(f_i)]^2\}/\sum_{i=1}^{N}\{[Re(\tilde{\chi}_{\text{data}_i})]^2 + [Im(\tilde{\chi}_{\text{data}_i})]^2\}$.

peak between 0.1 and 0.2 nm due to Pd–Cl interaction can be observed in this catalyst in all cases. No direct interaction between Pd and Cu can be observed. The coordination number of Pd–Cl was obtained by EXAFS fitting as shown in Table 3. There was no particular change in the coordination number due to Pd–Cl interaction and in the distance between palladium and chlorine as the nearest neighbor for different carbon-supported catalysts before and after the reaction at 353 K.

DISCUSSION

Effects of surface oxygen groups of carbon on the CO oxidation over carbon-supported Wacker-type catalysts were examined and the phase and the chemical environment of Pd and Cu species were observed.

In this study, FT-IR and TPD were used to characterize the surface oxygen groups. In the FT-IR study, we observed increased band intensities at 1000–1400, 1580, and 1750 cm^{-1} after treatment with an HNO_3 solution compared with untreated activated carbon. This is consistent with earlier reports (24–27). In general, the following assignment for IR bands could be made: a vibration of C=O in carboxyl groups at 1550–2050 cm^{-1}, –C=C– stretches at 1580 cm^{-1}, and C–O– vibrations at 1100–1450 cm^{-1}. The interpretation of peaks in TPD has also been developed. Otake and Jenkins (23) suggested that CO_2 desorption at low temperatures resulted from nonadjacent acidic oxygen complexes (carboxylic groups) formed at dangling carbon sites, and CO_2 desorption at high temperatures from adjacent acidic oxygen complexes (carboxylic anhydrides) formed at dangling carbon sites. They also reported that adjacent carboxylic anhydrides can be easily hydrolyzed in the presence of water and the resulting acidic proton can be replaced with cations. We observed that the peak representing carboxylic anhydrides is weakened after $PdCl_2$ and $CuCl_2$ are loaded. This can be interpreted as evidence of an interaction between these surface groups and catalyst precursors. Yamamoto *et al.* (13) observed a Cu(I) chloride species and a Pd(0) species over activated carbon-supported $PdCl_2$–$CuCl_2$ catalysts in XAFS study. They suggested that the surface functional groups worked as the reduction sites. Our TPD results could also be understood by considering an interaction between metal precursors and carbon supports. However, a reduced species such as Pd(0) or Cu(I) was never found in our catalysts. This difference in the electronic state of Pd and Cu explains the significantly higher activity of our catalyst system than that of Yamamoto *et al.* at low temperatures. Pd K-edge XAFS results suggest that Pd is present as a molecular Pd(II) species coordinated with chlorine ion in all catalysts. This justifies our definition of the turnover rate because the dispersion of Pd would be 1 in this case. The XAFS characterization of WA-1 and WA-2 that have quite different surface properties shows that the structural and electronic states of palladium species of both catalysts are almost the same. Recently, the addition of $Cu(NO_3)_2$ as an additional copper precursor was reported to decrease the coordination number of Pd–Cl to a certain degree (16). The same trend was also observed between WA-1 and WA-3 or WA-2 and WA-4. There, molecular palladium species still remain largely unchanged before and after the reaction at 353 K. Similarly to the case WA-1 and WA-2, we could not find a difference in the coordination numbers of Pd–Cl for WA-3 and WA-4 even though surface properties were quite different (data not shown). Therefore, the surface modification of carbon does not change the structural and electronic states of palladium species noticeably.

We studied the effects of the copper phase on CO oxidation over supported Wacker-type catalysts and reported that the XRD intensity of the $Cu_2Cl(OH)_3$ phase of a catalyst was closely correlated with its catalytic activity (15). Similarly, we could observe the formation of a well-defined copper solid phase, $Cu_2Cl(OH)_3$, in XRD patterns, for highly active catalysts such as WA-3 and WA-4. The higher peak intensity for WA-4, whose surface has a higher population of functional groups than that of WA-3, also supports the assumption that this copper phase is formed by an interaction between the copper precursor and the surface functional groups. The overall chemistry of CO oxidation in this catalytic system is believed to be similar to that of the well-known Wacker process in the presence of a homogeneous $PdCl_2$–$CuCl_2$ catalyst (6). Thus, initially the Pd(II) species is reduced to Pd(0) by carbon monoxide, and then Pd(0) is reoxidized to Pd(II) species by a Cu(II) compound which is reduced during this process into Cu(I) species and then is reoxidized to Cu(II) compounds by molecular O_2 included in the feed gas stream. In this process, the $Cu_2Cl(OH)_3$ phase is believed to perform better than other copper phases for the reoxidation of reduced Pd(0) into Pd(II) species due to its easier reducibility (18). Comparing WA-2 and WA-3, the addition of $Cu(NO_3)_2$ in the preparation step seemed more effective for the formation of a $Cu_2Cl(OH)_3$ phase than the acid treatment as shown in Fig. 7.

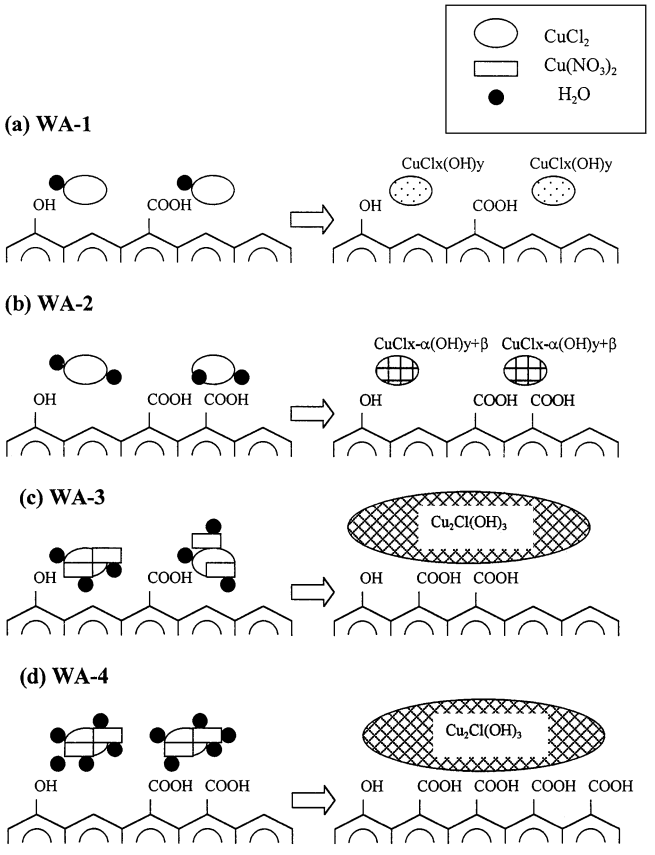

FIG. 11. Schematics of the transformation of copper phase and surface functional groups during the reaction.

A schematic representation of the transformation of the copper phase for WA-1 to WA-4 during reaction is shown in Fig. 11. As indicated by FT-IR and TPD in Figs. 1 and 2, more surface functional groups are present in WA-2 and WA-4 than in WA-1 and WA-3 due to the nitric acid treatment. These groups increase hydrophilicity, which helps in the adsorption of a greater amount of water around copper species in the preparation step. As a reaction goes on, the acidic surface functional groups and water interact with copper species and then hydroxyl ion is incorporated with Cu(II) and chlorine ion around Cu(II) is removed as HCl. Thus, more hydroxide ligand and less chloride ligand could be present around Cu(II) over WA-2 than over WA-1, and the hydroxide could attack the crystalline $CuCl_2 \cdot 2H_2O$ phase. As shown in Fig. 7B, the peak representing the $CuCl_2 \cdot 2H_2O$ phase in XRD patterns was weaker for WA-2 than for WA-1 after the reaction. To support these structural changes around copper over different supports before and after a reaction, Cu K-edge EXAFS spectra of WA-1 and WA-2 before and after the reaction at 353 K were obtained. Their radial structural functions (RSFs) are displayed in Fig. 12. For all cases, two major peaks between 0.1 nm and 0.2 nm were found in the first shell. Compared with reference samples, peaks at 0.15 nm and 0.18 nm (without phase corrections) can be assigned to Cu–O and Cu–Cl interactions, respectively. Since there are several contributions from oxygen at different distances (33, 34), the quantitative EXAFS fitting could not be accomplished successfully. However, noticeable differences have been observed in the peak representing Cu–Cl interactions. Compared with WA-2, WA-1 has a stronger peak

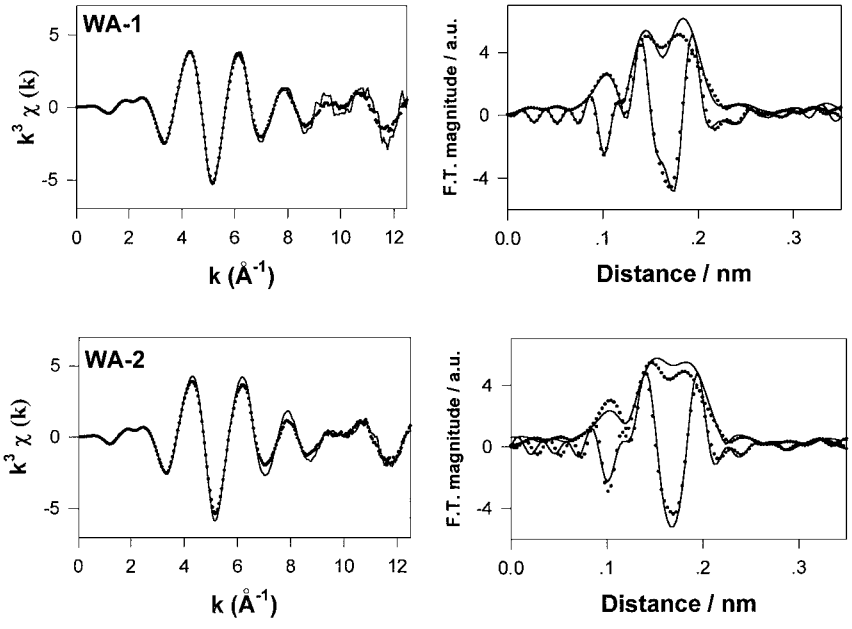

FIG. 12. k^3-weighted EXAFS functions and their Fourier transformation about the Cu K-edge of WA-1 and WA-2 before (solid line) and after the reaction at 353 K (dotted line).

intensity at 0.18 nm before the reaction, which can be interpreted as evidence that more chlorine ion is coordinated into copper for WA-1 catalyst than for WA-2 catalyst. For all cases, the peak representing a Cu–Cl interaction weakened after the reaction at 353 K. This loss of chlorine ion during the reaction accompanies increasing activity at the initial stage as shown in Fig. 3b. This is also closely related to the fact that $Cu_2Cl(OH)_3$ is more effective than $CuCl_2 \cdot 2H_2O$. The former has the smaller number of chlorine ions around copper than the latter. However, in the absence of chlorine ion, the active Pd(II) was reported to be reduced to Pd(0) irreversibly (16). Therefore, the smaller number of chlorine ligand around copper may give a higher activity although its existence is essential for the redox cycle of the Wacker chemisty.

For WA-3 and WA-4 containing $Cu(NO_3)_2$ as an additional copper precursor, the irregular agglomeration of $CuCl_2$ and $Cu(NO_3)_2$ is present in the initial stage, which is supported by the invisible crystalline copper phase in XRD as shown in Fig. 7A. WA-4 catalysts containing more surface functional groups can adsorb more water molecules around copper species than WA-3 catalysts. As the reaction goes on, the amorphous solid mixture of $Cu(NO_3)_2$ and $CuCl_2$ transforms into crystalline $Cu_2Cl(OH)_3$ as shown in Fig. 7B. As in the case of WA-1 and WA-2, surface functional groups and water molecules help this chlorine removal and hydroxide addition around Cu(II). $Cu(NO_3)_2$ also promotes the formation of surface oxygen groups. As discussed elsewhere (24), the nitric acid oxidation of activated carbons may have some analogies to the oxidation of aromatic hydrocarbons. The oxidation reaction is thought to proceed by a radical mechanism. In this reaction, $\cdot NO_2$ plays a key role in the activation of hydrocarbons. Therefore, $\cdot NO_2$ radical produced from $Cu(NO_3)_2$ during its transformation into $Cu_2Cl(OH)_3$ may oxidize the surface aromatic carbon rings and be reduced into NO which was detected during TPD as shown in Fig. 5c.

The presence of water is essential to sustain this catalytic cycle of Wacker chemistry, and this was also found experimentally to be so for supported Wacker-type catalysts (9). The supported Wacker-type catalysts have been reported to have an unusual temperature dependence of their catalytic activity showing a maximum around room temperature and decreasing with increasing reaction temperatures (14). In this work, lower CO oxidation rates were obtained at 353 K than at 313 K for WA-1 catalyst as shown in Fig. 3. As the reaction temperature increases, the reaction rate constant increases but the amount of adsorbed water decreases to a level where the formation of the aqueous phase is difficult. From the H_2O-TPD experiment, we observed that the HNO_3-treated carbon adsorbed a greater amount of H_2O on its surface than untreated carbon. This hydrophilicity may be responsible for the higher activity of WA-2 compared with that of WA-1. This tendency was confirmed in

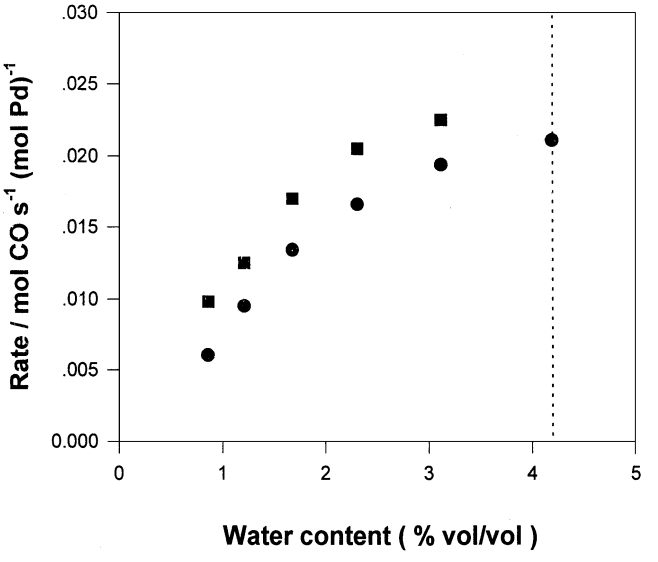

FIG. 13. Effect of water content on CO oxidation activities over WA-1 (●) and WA-2 (■) at 303 K. The reactants, CO (1 vol%) and O_2 (10 vol%), in N_2 were saturated with water at different temperatures and fed to the catalysts.

Fig. 13 where the effect of water on CO oxidation activity was compared for WA-1 and WA-2 catalysts. As mentioned above, WA-2 showed superior activity compared to that of WA-1 at the same water content in feed. At 100% relative humidity (as shown by the dashed line in Fig. 13), however, WA-2 showed decreasing rate with reaction time and the steady-state activity could not be obtained. However, a steady-state activity was obtained for WA-1 as indicated in Fig. 13. The decreasing activity for WA-2 is believed to be due to the complete pore-filling, which results in the reduction in effective contact area between gaseous reactants and the catalyst(7).

One thing should be mentioned about sulfur contents in carbon supports. Sulfur contents of 0.73 wt% and 0.04 wt% were determined in the fresh activated carbon and the modified activated carbon, respectively. From XRD and XAFS studies; however, no evidence of incorporation of sulfur into palladium or copper was observed. Therefore, the existence of sulfur seems to have no significant effect on the catalyst system. However, the presence of SO_2 in a feed stream was reported to deactivate this catalyst system (15).

CONCLUSIONS

The surface of active carbon used to prepare supported Wacker-type catalysts is enriched with carboxylic and carbonyl groups by the pretreatment with HNO_3 or the addition of $Cu(NO_3)_2$ as an additional copper precursor. These surface groups increase the hydrophilicity and promote the formation of an active copper phase, $Cu_2Cl(OH)_3$. When $Cu(NO_3)_2$ is present together with $CuCl_2$ as catalyst

precursors, the effects are greater, especially that on the formation of $Cu_2Cl(OH)_3$. The formation of the active copper phase and the enhanced hydrophilicity appear to be responsible for the increased rate of CO oxidation.

REFERENCES

1. Smidt, J. R., Hafner, W., Jira, R., Sedlmeier, J., Sieber, R., Ruttinger, R., and Kojer, H., *Angew. Chem.* **71**, 176 (1959).
2. Miller, S. A., Ed., "Ethylene and Its Industrial Derivatives," p. 658. Ernest Benn, London, 1969.
3. Evnin, A. B., Rabo, J. A., and Kasai, P. H., *J. Catal.* **30**, 109 (1973).
4. Rao, V., and Datta, R., *J. Catal.* **114**, 377 (1988).
5. Lloyd, W. G., and Rowe, D. R., *Environ. Sci. Technol.* **5**(11), 1133 (1971).
6. Desai, M. N., Butt, J. B., and Dranoff, J. S., *J. Catal.* **79**, 95 (1983).
7. Choi, K. I., and Vannice, M. A., *J. Catal.* **127**, 489 (1991).
8. Lee, C. W., Park, S.-J., Kim, Y.-S., and Chong, P. J., *Bull. Korean Chem. Soc.* **16**(3), 296 (1995).
9. Kim, K. D., Nam, I.-S., Chung, J. S., Lee, J. S., Ryu, S. G., and Yang, Y. S., *Appl. Catal. B* **5**, 103 (1994).
10. Lloyd, W. G., and Rowe, D. R., U.S. Patent 3,790,662 (1974).
11. Lee, J. S., Choi, S. H., Kim, K. D., and Nomura, M., *Appl. Catal. B* **7**, 199 (1996).
12. Choi, S. H., and Lee, J. S., *React. Kinet. Catal. Lett.* **57**, 227 (1996).
13. Yamamoto, Y., Matsuzaki, T., Ohdan, K., and Okamoto, Y., *J. Catal.* **161**, 577 (1996).
14. Koh, D. J., Song, J. H., Ham, S.-W., Nam, I.-S., Chang, R.-W., Park, E. D., Lee, J. S., and Kim, Y. G., *Korean J. Chem. Eng.* **14**(6), 486 (1997).
15. Park, E. D., and Lee, J. S., *J. Catal.* **180**, 123 (1998).
16. Park, E. D., and Lee, J. S., *Stud. Surf. Sci. Catal.*, in press.
17. Lee, J. S., Park, E. D., and Song, B. J., *Catal. Today* **54**, 57 (1999).
18. Rouco, A. J., *J. Catal.* **157**, 380 (1995).
19. Zipelli, C., Bart, J. C., Petrini, G., Galvagno, S., and Cimino, C. Z., *Anorg. Allg. Chem.* **502**, 199 (1983).
20. Kinoshita, K., "Carbon: electrochemical and Physicochemical Properties." Wiley-Interscience, New York, 1988.
21. Rivin, D., *Rubber Chem. Technol.* **44**, 307 (1971).
22. Coltharp, M. T., and Hackerman, N., *J. Phys. Chem.* **72**, 1171 (1968).
23. Otake, Y., and Jenkins, R. G., *Carbon* **31**(1), 109 (1993).
24. Vinke, P., van der Eijk, M., Verbree, M., Voskamp, A. F., and van Bekkum, H., *Carbon* **32**(4), 675 (1994).
25. Fanning, P. E., and Vannice, M. A., *Carbon* **31**(5), 721 (1993).
26. Dandekar, A., Baker, R. T. K., and Vannice, M. A., *Carbon* **36**(12), 1821 (1998).
27. Dandekar, A., Baker, R. T. K., and Vannice, M. A., *J. Catal.* **183**, 131 (1999).
28. Stern, E. A., Newville, M., Ravel, B., Yacoby, Y., and Haskel, D., *Physica B* **208**&**209**, 117 (1995).
29. Rehr, J. J., Mustre de Leon, J., Zabinsky, S. I., and Albers, R. C., *J. Am. Chem. Soc.* **113**, 5135 (1991).
30. Teo, B. K., "EXAFS: Basic Principles and Data analysis." Springer, Berlin, 1985.
31. Wells, A. F., "Structural Inorganic Chemistry," 5th ed. Clarendon Press, Oxford, 1984.
32. Wells, A. F., *Kristallogr.* **100**, 189 (1938).
33. Leofanti, G., Padovan, M., Garilli, M., Carmello, D., Zecchina, A., Spoto, G., Bordiga, S., Turnes Palomino, G., and Lamberti, C., *J. Catal.* **189**, 91 (2000).
34. Leofanti, G., Padovan, M., Garilli, M., Carmello, D., Marra, G. L., Zecchina, A., Spoto, G., Bordiga, S., and Lamberti, C., *J. Catal.* **189**, 105 (2000).